Available online at www.sciencedirect.com
SCIENCE DIRECT®
Fluid Phase Equilibria 221 (2004) 63–72
FLUID PHASE EQUILIBRIA
www.elsevier.com/locate/fluid

Square-well chain molecules: a semi-empirical equation of state and Monte Carlo simulation data

Ming-Jer Lee [a,*], Clare McCabe [b], Peter T. Cummings [c,d]

[a] *Department of Chemical Engineering, National Taiwan University of Science and Technology, 43 Keelung Road, Section 4, Taipei 106-07, Taiwan*
[b] *Department of Chemical Engineering, Colorado School of Mines, Golden, CO 80401, USA*
[c] *Department of Chemical Engineering, Vanderbilt University, Nashville, TN, USA*
[d] *Chemical Sciences Division, Oak Ridge National Laboratory, Oak Ridge, TN, USA*

Received 3 October 2003; accepted 5 March 2004

Available online 20 June 2004

Abstract

A semi-empirical equation of state was developed for square-well chain fluids on the basis of Monte Carlo (MC) simulation data. The equation was formed by combining terms describing non-bonded square-well segments, hard-sphere chain formation, and a perturbation term describing the square-well contribution to chain formation. The functional dependence on the chain length is the same as that derived in the statistical associating fluid theory (SAFT). Extensive isobaric–isothermal MC simulations were performed for the dimer, 4-mer, 8-mer, and 16-mer square-well fluids at temperatures below or near the critical point. The new equation satisfactorily represents the volumetric properties of square-well chain fluids, up to and including the 100-mer, which was the longest chain length studied. Additionally, the new model accurately reproduces the phase envelopes of the dimer and 4-mer fluids, however, it underestimates the vapor pressures for 8-mer's and above.

Keywords: Square well; Simulation; Equation of state; SAFT-VR

1. Introduction

The development of an accurate equation of state for chain molecules is theoretically and practically important. To gain insight into the microscopic and macroscopic behavior of chain molecules, many investigators have performed molecular simulations for various model chain fluids, such as hard-sphere chains [1–7], square-well chains [8–22], Lennard-Jones chains [14], and Yukawa chains [23–25]. Among these chain fluids, the square-well chain fluid is the simplest one having both repulsive and attractive parts. Additionally, the potential model has four parameters (chain length m, hard core diameter σ, characteristic attraction energy ε, and dimensionless well width λ), resulting in significant flexibility when fitting to experimental data. Furthermore, the properties of the square-well fluid can be found accurately from perturbation theory in terms of hard sphere reference states.

Simulation studies of these model fluids provide valuable information from which it is possible to develop equations of state for real molecules. In recent years, the statistical associating fluid theory (SAFT) [26,27] and its many variations [28] have been successfully applied to calculate thermodynamic properties of both model chain molecules and real experimental systems of small molecules, polymeric materials, and their mixtures [29]. In SAFT and related molecular-based equations of state [26,27,30–39], the perturbation theories of Barker and Henderson [40] and Wertheim [41–44] have been widely adopted to represent the reference unbonded (or monomer) segments and bond formation for square-well chain molecules. One of the impediments to the more widespread adoption of SAFT-derived equations of state for process simulation is perceived the complexity of the association term and resulting computational expense. In the present study, a simple semi-empirical equation of state is developed on the basis of MC simulation data for square-well chain molecules. The single

* Corresponding author. Tel.: +886-2-2737-6626; fax: +886-2-2737-6644.
E-mail address: mjl@ch.ntust.edu.tw (M.-J. Lee).

0378-3812/$ – see front matter © 2004 Elsevier B.V. All rights reserved.
doi:10.1016/j.fluid.2004.03.008

closed-form mathematical expression obtained should ensure its usefulness in process calculations.

In the last decade, several MC simulation studies for square-well chain fluids and their mixtures have been reported in the literature. For pure square-well chain fluids *PVT* properties [9–11,13,14], vapor–liquid equilibrium (VLE) phase envelopes [8,14,17], second virial coefficients [12], configurational internal energy [15], and constant-volume heat capacity [19] data are available. For square-well chain mixtures, Gulati and Hall [16] and Paredes et al. [19] calculated *PVT* properties and configurational internal energy, Davies et al. [17] computed the VLE properties for mixtures of square-well monomers and dimers, while McCabe et al. [45] studied non-conformal monomer—dimer mixtures. However, despite this body of data, the volumetric properties of square-well chain molecules at conditions below or near the critical temperatures are rather limited. Consequently, in the present study, MC simulations in the isothermal–isobaric (NPT) ensemble have been performed for the dimer, 4-mer, 8-mer, and 16-mer fluids to obtain a more complete description of the *PVT* behavior.

2. Monte Carlo simulations

We have calculated the *PVT* behaviour and structure of the dimer, tetramer, 8-mer and 16-mer square-well fluids using NPT MC simulation. The simulations were performed with systems of $N = 128$ for the dimer and 16-mer fluids and $N = 256$ for the 4-mer and 8-mer fluids. Initial configurations were generated at low pressure by arranging the molecules on a face-centred-cubic lattice. Simulations at higher pressure, and hence density, were then started from this equilibrated initial configuration and allowed to re-equilibrate to the corresponding density.

One simulation cycle consisted of N attempted displacement, reorientation and reptation moves (i.e. the same number of MC moves as the total number of molecules in the system), one attempted volume change, and a specific number of attempted re-growths of randomly selected molecules using continuum configurational bias sampling (CCB) [46]. CCB was used in the reptation and re-growth moves for N-mers greater than $N = 4$. In all the simulations the maximum displacement and volume change was adjusted to give an acceptance ratio of between 30 and 40%, and the number of re-growths controlled so that between 1 and 3% of the molecules are re-grown each cycle. The thermodynamic properties of the system were obtained as ensemble averages and the errors estimated by determining the standard deviation. An initial simulation of 10^6 cycles was performed to equilibrate the system, depending upon pressure and chain length, before averaging for between 10^6 and 2×10^6 cycles. As can be seen from Table 1, the agreement between the results obtained in this study and literature values is within the uncertainties of the computations. Having validated the code we then performed simulations at reduced temperatures (T^*) from 0.6 to 1.85 for the dimer fluid, from 1.3 to 2.0 for the 4-mer, and from 1.5 to 2.0 for the 8-mer and 16-mer fluids. The reduced pressures (P^*) are in the range of 0.0006 up to 3.0 for all systems. In addition to $\lambda = 1.5$, simulations were also performed with different values of the well-width, from $\lambda = 1.275$ to $\lambda = 1.725$ for the dimer and 4-mer fluids.

3. Simulation results

In this study, simulations at 134 state conditions have been performed. Tables 2–5 list the simulation results for the dimer, 4-mer, 8-mer, and 16-mer fluids, respectively. The *PVT* diagrams are presented in Figures 1–4. We note from the figures that the results from different investigators appear to be consistent, except for the isotherm at $T^* = 2.0$ for the 4-mer near the critical region ($P^* = 0.07$–0.12). Figure 2 shows that our results are located in between those of Yethiraj and Hall [9] and Taveres et al. [13].

We have also studied the effect of the well-width for the square-well potential on the volumetric properties. Figures 5 and 6 illustrate, respectively, the *PVT* properties of the dimer and 4-mer fluids with λ ranging from 1.275 to

Table 1
Comparison of the results with literature values

	T^*	P^*	η	Uncertainty	N	Note
Dimer	2.0	1.0998	0.314	0.001	128 × 2	This work
	2.0	1.0998	0.3142		256	Tavares et al. [13]
4-Mer	2.0	0.46	0.309	0.001	256 × 2	This work
	2.0	0.46	0.309			Escobedo and de Pablo [14]
	2.0	4.96	0.426	0.001	256 × 2	This work
	2.0	4.96	0.428			Escobedo and de Pablo [14]
8-Mer	2.5	0.2	0.230	0.001	256 × 2	This work
	2.5	0.2	0.234			Escobedo and de Pablo [14]
16-Mer	4.0	2.45865	0.313	0.002	128 × 2	This work
	4.0	2.45865	0.31416		70	Tavares et al. [13]

Results are given in terms of reduced units: $T^* = kT/\varepsilon$, $P^* = P\sigma^3/\varepsilon$, and $\eta = (\pi/6)\rho\sigma^3$ where ρ is the segment number density.

Table 2
Simulation results for square-well dimer fluid

T^*	P^*	η	Uncertainty	Z	λ
0.6	0.001	0.453	0.001	0.004	1.5
	0.05	0.455	0.001	0.192	1.5
	0.1	0.457	0.001	0.383	1.5
	0.5	0.467	0.001	1.869	1.5
	1.5	0.486	0.001	5.387	1.5
	3.0	0.510	0.001	10.267	1.5
0.8	0.001	0.425	0.001	0.003	1.5
	0.05	0.426	0.001	0.154	1.5
	0.1	0.428	0.001	0.306	1.5
	0.5	0.437	0.001	1.498	1.5
	1.5	0.458	0.001	4.287	1.5
	3.0	0.483	0.001	8.130	1.5
1.0	0.02	0.397	0.001	0.053	1.5
	0.05	0.398	0.001	0.132	1.5
	0.1	0.400	0.001	0.262	1.5
	0.5	0.412	0.001	1.271	1.5
	1.5	0.436	0.001	3.603	1.5
	3.0	0.460	0.001	6.830	1.5
1.2	0.05	0.365	0.001	0.120	1.5
	0.1	0.368	0.001	0.237	1.5
	0.5	0.386	0.001	1.130	1.5
	1.5	0.413	0.001	3.169	1.5
	3.0	0.441	0.001	5.937	1.5
1.4	0.05	0.315	0.001	0.119	1.5
	0.1	0.325	0.002	0.230	1.5
	0.5	0.357	0.001	1.048	1.5
	1.5	0.394	0.001	2.848	1.5
	3.0	0.424	0.001	5.292	1.5
1.5	0.07	0.289	0.003	0.169	1.5
	0.1	0.295	0.001	0.237	1.5
1.65	0.05	0.047	0.001	0.675	1.5
	0.06	0.061	0.005	0.624	1.5
	0.07	0.074	0.005	0.600	1.5
	0.08	0.117	0.005	0.434	1.5
	0.09	0.171	0.017	0.334	1.5
	0.1	0.200	0.008	0.317	1.5
	0.2	0.272	0.001	0.467	1.5
	0.5	0.318	0.001	0.998	1.5
	1.5	0.367	0.001	2.594	1.5
	3.0	0.403	0.001	4.725	1.5
1.85	0.05	0.035	0.002	0.809	1.5
	0.1	0.082	0.001	0.690	1.5
	0.2	0.198	0.001	0.572	1.5
	0.5	0.280	0.001	1.011	1.5
	1.5	0.348	0.001	2.440	1.5
	3.0	0.388	0.001	4.377	1.5
1.4	0.05	0.038	0.001	0.984	1.275
	0.5	0.256	0.001	1.461	1.275
	1.5	0.367	0.001	3.057	1.275
	3.0	0.424	0.001	5.292	1.275
1.4	0.05	0.373	0.001	0.100	1.725
	0.5	0.389	0.001	0.961	1.725
	1.5	0.412	0.001	2.723	1.725
	3.0	0.438	0.001	5.123	1.725
1.85	0.05	0.027	0.001	1.048	1.275
	0.1	0.053	0.001	1.068	1.275
	0.5	0.184	0.001	1.538	1.275
	3.0	0.371	0.001	4.577	1.275
1.85	0.05	0.320	0.001	0.088	1.725
	0.1	0.323	0.001	0.175	1.725
	0.5	0.341	0.001	0.830	1.725
	3.0	0.402	0.001	4.224	1.725

Table 3
Simulation results for square-well 4-mer fluid

T^*	P^*	η	Uncertainty	Z	λ
1.3	0.001	0.380	0.001	0.004	1.5
	0.02	0.381	0.001	0.085	1.5
	0.05	0.381	0.002	0.211	1.5
	0.1	0.384	0.001	0.420	1.5
	0.5	0.399	0.001	2.019	1.5
	1.5	0.424	0.001	5.700	1.5
	3.0	0.450	0.001	10.741	1.5
1.5	0.02	0.345	0.001	0.081	1.5
	0.05	0.348	0.002	0.201	1.5
	0.1	0.353	0.001	0.396	1.5
1.7	0.05	0.303	0.003	0.203	1.5
	0.1	0.312	0.001	0.395	1.5
	0.5	0.351	0.001	1.755	1.5
	1.5	0.390	0.001	4.738	1.5
	3.0	0.419	0.001	8.821	1.5
1.8	0.03	0.233	0.008	0.150	1.5
	0.05	0.270	0.003	0.215	1.5
	0.1	0.287	0.003	0.405	1.5
	0.5	0.338	0.001	1.721	1.5
	1.5	0.380	0.001	4.593	1.5
	3.0	0.412	0.001	8.472	1.5
1.9	0.03	0.078	0.010	0.424	1.5
	0.05	0.193	0.002	0.286	1.5
	0.1	0.253	0.002	0.436	1.5
	0.5	0.325	0.001	1.696	1.5
	1.0	0.355	0.001	3.105	1.5
2.0	0.03	0.049	0.001	0.641	1.5
	0.05	0.107	0.001	0.489	1.5
	0.07	0.175	0.005	0.419	1.5
	0.1	0.217	0.004	0.483	1.5
	0.3	0.288	0.001	1.091	1.5
	0.5	0.312	0.001	1.678	1.5
1.7	0.05	0.054	0.001	1.141	1.275
	0.5	0.254	0.001	2.425	1.275
	3.0	0.410	0.001	9.015	1.275
1.7	0.05	0.372	0.001	0.166	1.725
	0.5	0.386	0.001	1.596	1.725
	3.0	0.433	0.001	8.536	1.725
2.0	0.05	0.045	0.001	1.164	1.275
	0.5	0.214	0.001	2.447	1.275
	3.0	0.382	0.001	8.224	1.275
2.0	0.05	0.346	0.001	0.151	1.725
	0.5	0.363	0.001	1.442	1.725
	3.0	0.412	0.001	7.625	1.725

1.725. From the figures we note that the isotherms have a strong dependence on λ, especially in the vicinity of critical point.

4. Equation of state for square-well chain molecules

A new equation of state for square-well chain molecules was derived by summing the contributions from non-bonded square-well segments, $Z_{sw,nb}$, and chain formation for

Table 4
Simulation results for square-well 8-mer fluid

T^*	P^*	η	Uncertainty	Z	λ
1.5	0.0006	0.369	0.001	0.005	1.5
	0.02	0.370	0.001	0.151	1.5
	0.05	0.372	0.002	0.375	1.5
	0.1	0.375	0.001	0.743	1.5
	1.0	0.406	0.001	6.878	1.5
1.7	0.003	0.334	0.003	0.022	1.5
	0.02	0.338	0.001	0.146	1.5
	0.05	0.341	0.002	0.361	1.5
	0.1	0.345	0.001	0.714	1.5
	0.5	0.370	0.001	3.330	1.5
	1.5	0.402	0.001	9.194	1.5
	3.0	0.430	0.001	17.191	1.5
1.9	0.005	0.287	0.004	0.038	1.5
	0.02	0.292	0.005	0.151	1.5
	0.05	0.299	0.001	0.369	1.5
	0.1	0.311	0.001	0.709	1.5
	0.5	0.349	0.001	3.158	1.5
	1.5	0.387	0.001	8.545	1.5
	3.0	0.416	0.001	15.899	1.5
2.0	0.008	0.249	0.002	0.067	1.5

square-well molecules, $Z_{sw,cf}$:

$$Z = Z_{sw,nb} + Z_{sw,cf} \quad (1)$$

For square-well chain molecules with m segments, Z is defined as

$$Z = \frac{\pi P^* m}{6T^*\eta} \quad (2)$$

where $P^* = P\sigma^3/\varepsilon$, $T^* = kT/\varepsilon$, η is the reduced density ($=\pi\sigma^3\rho/6$), and ρ the number density of segments.

Table 5
Simulation results for square-well 16-mer fluid

T^*	P^*	η	Uncertainty	Z	λ
1.5	0.003	0.379	0.002	0.044	1.5
	0.02	0.379	0.001	0.295	1.5
	0.05	0.382	0.001	0.731	1.5
	0.1	0.383	0.001	1.458	1.5
	3.0	0.428	0.001	39.148	1.5
1.7	0.003	0.350	0.003	0.042	1.5
	0.02	0.351	0.001	0.281	1.5
	0.05	0.356	0.001	0.692	1.5
	0.1	0.362	0.002	1.361	1.5
	0.5	0.381	0.001	6.467	1.5
	1.5	0.405	0.001	18.252	1.5
	3.0	0.424	0.002	34.868	1.5
2.0	0.003	0.295	0.002	0.043	1.5
	0.02	0.300	0.001	0.279	1.5
	0.05	0.304	0.002	0.689	1.5
	0.1	0.314	0.001	1.334	1.5
	0.5	0.347	0.001	6.036	1.5

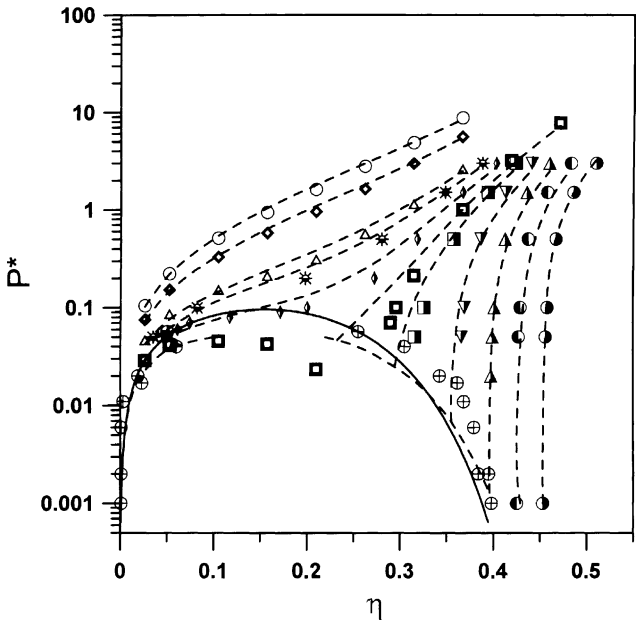

Figure 1. *PVT* diagram for square-well dimer fluid at $T^* = 0.6$ (◑), $T^* = 0.8$ (◐), $T^* = 1.0$ (◭), $T^* = 1.2$ (▽), $T^* = 1.4$ (□), $T^* = 1.5$ (◘)) [13], $T^* = 1.65$ (◊), $T^* = 1.85$ (✳), $T^* = 2.0$ (△) [13], $T^* = 3.0$ (◇) [13] and $T^* = 4.0$ (○) [13]. Also shown are the vapor–liquid coexisting points (⊕) [17], calculated results from the SAFT-VR equation (solid line) and the new equation of state (dashed line).

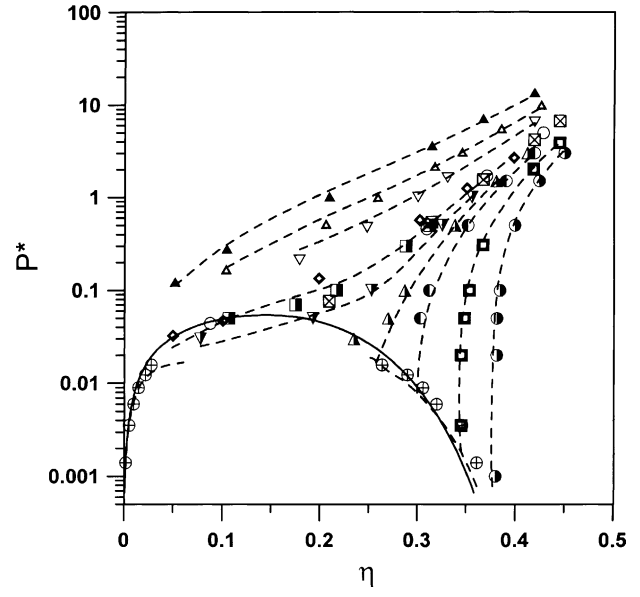

Figure 2. *PVT* diagram for square-well 4-mer fluid at $T^* = 1.3$ (◑), $T^* = 1.5$ (◘) [13], $T^* = 1.7$ (◐), $T^* = 1.8$ (◭), $T^* = 1.9$ (▽), $T^* = 2.0$ (⊠) [13], $T^* = 2.0$ (◇) [9], $T^* = 2.0$ (○) [14], $T^* = 2.0$ (◨), $T^* = 2.5$ (▽) [14], $T^* = 3.0$ (△) [14] and $T^* = 4.0$ (▲) [13]. Also shown are the vapor–liquid coexisting points (⊕) [14], calculated results from the SAFT-VR equation (solid line) and the new equation of state (dashed line).

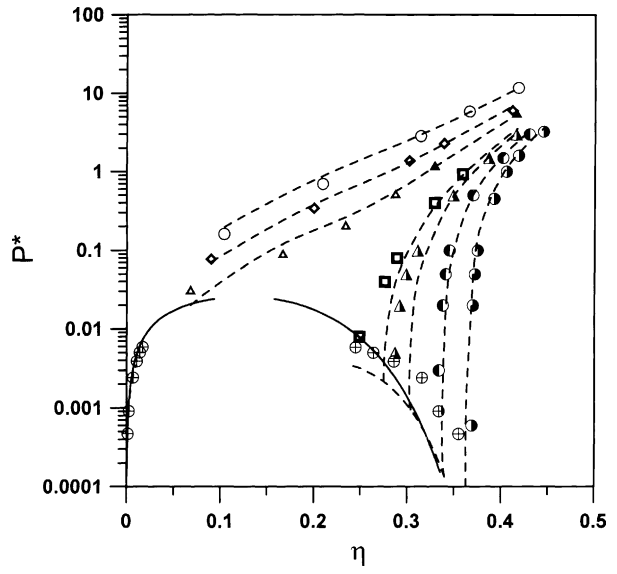

Figure 3. *PVT* diagram for square-well 8-mer fluid at $T^* = 1.5$ (◑) [13], $T^* = 1.7$ (◐), $T^* = 1.9$ (◭), $T^* = 2.0$ (◘) [14], $T^* = 2.5$ (△) [14], $T^* = 3.0$ (◆) [13] and $T^* = 4.0$ (○) [13]. Also shown are the vapor–liquid coexisting points (⊕) [14], calculated results from the SAFT-VR equation (solid line) and the new equation of state (dashed line).

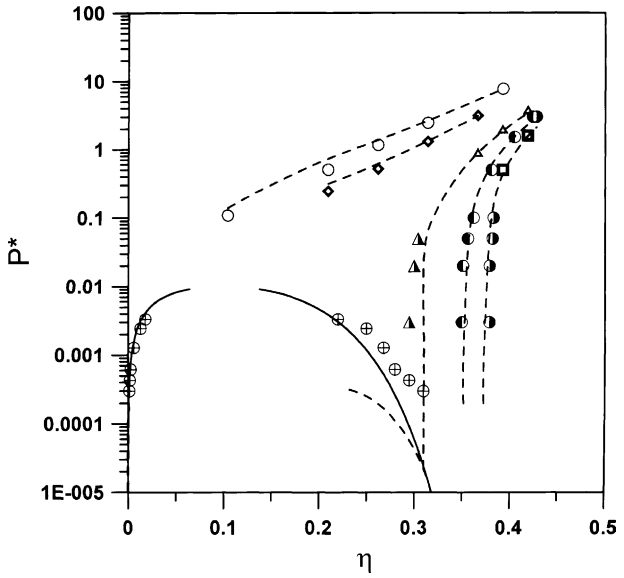

Figure 4. *PVT* diagram for square-well 16-mer fluid at $T^* = 1.5$ (◘) [13], $T^* = 1.5$ (◑), $T^* = 1.7$ (◐), $T^* = 2.0$ (△) [13], $T^* = 2.0$ (◭), $T^* = 3.0$ (◆) [13] and $T^* = 4.0$ (○) [13]. Also shown are the vapor–liquid coexisting points (⊕) [14], calculated results from the SAFT-VR equation (solid line) and the new equation of state (dashed line).

4.1. Contribution of non-bonded square-well segments

For a square-well chain molecule with m segments, the compressibility factor of non-bonded square-well segments is expressed as

$$Z_{\mathrm{sw,nb}} = 1 + m[(Z_{\mathrm{hs}} - 1) + Z_{\mathrm{sw,att}}] \tag{3}$$

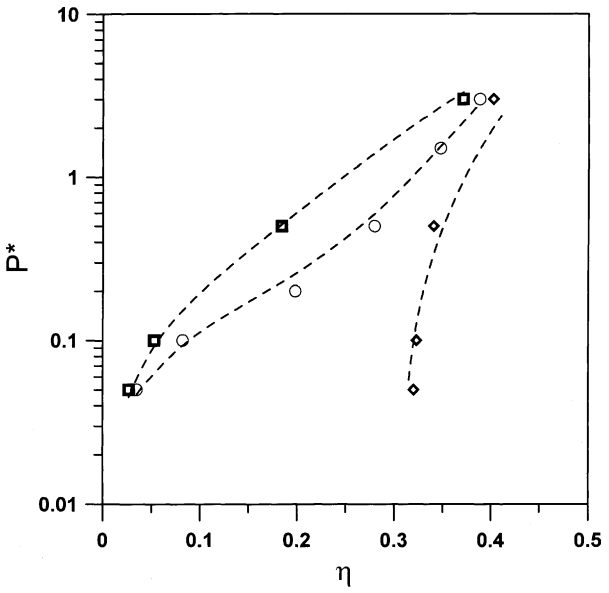

Figure 5. Volumetric properties of square-well dimer fluid at $T^* = 1.85$ and $\lambda = 1.275$ (◘); $\lambda = 1.5$ (○); $\lambda = 1.725$ (◆). Dashed lines are the calculated results from the new equation of state.

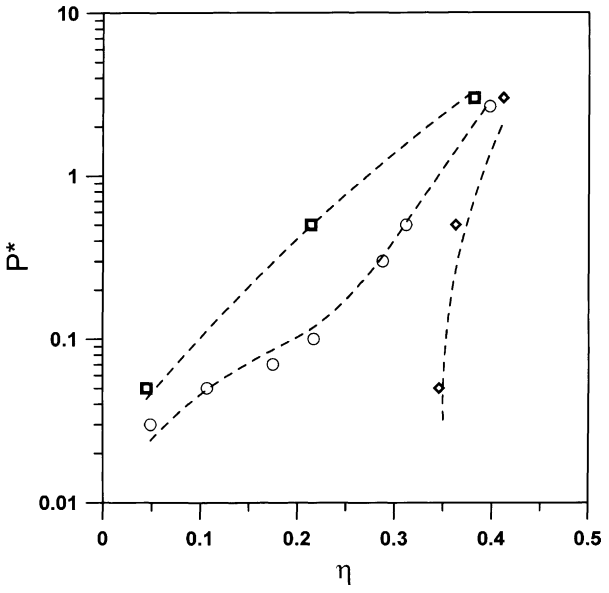

Figure 6. Volumetric properties of square-well 4-mer fluid at $T^* = 2.0$ and $\lambda = 1.275$ (◘); $\lambda = 1.5$ (○); $\lambda = 1.725$ (◆). Dashed lines are the calculated results from the new equation of state.

where Z_{hs} and $Z_{\mathrm{sw,att}}$ are the compressibility factors of hard-sphere molecules and attractive contribution of square-well monomers, respectively. Lin et al. [47] have developed simple expressions for representation of Z_{hs} and $Z_{\mathrm{sw,att}}$:

$$Z_{\mathrm{hs}} = \frac{1 + k_1\eta}{1 - k_2\eta} \tag{4}$$

and

$$Z_{\mathrm{sw,att}} = (\lambda - 0.5)^{3/2}\left[\frac{k_6\eta + k_7\eta^2}{T^*(1 - k_2\eta)(1 - k_3\eta)}\right] \tag{5}$$

Table 6
PVT data used in the parameter estimation

	T^*	P^*	λ	N	Source
Dimer	0.6–1.85	0.001–3.0	1.275–1.725	62	This work
	1.0–1.46	P^{sat}	1.5	12	Davies et al. [17]
	1.5–4.0	0.029–27.938	1.5	54	Tavares et al. [13]
				128	
4-Mer	1.3–2.0	0.001–3.0	1.275–1.725	44	This work
	2.0–3.0	0.044–9.611	1.5	16	Escobedo and de Pablo [14]
	1.5–3.0	0.033–5.582	1.5	12	Yethiraj and Hall [9]
	1.4–1.75	P^{sat}	1.5	12	Escobedo and de Pablo [14]
	1.5–4.0	0.007–13.061	1.5	22	Tavares et al. [13]
				106	
8-Mer	1.5–2.0	0.0006–3.0	1.5	20	This work
	2.0–3.0	0.03–7.505	1.5	14	Escobedo and de Pablo [14]
	2.0–3.0	0.077–6.028	1.5	7	Yethiraj and Hall [9]
	1.6–1.97	P^{sat}	1.5	12	Escobedo and de Pablo [14]
	1.5–4.0	0.161–11.793	1.5	16	Tavares et al. [13]
				69	
16-Mer	1.5–2.0	0.003–3.0	1.5	17	This work
	3.0	0.055–4.837	1.5	4	Yethiraj and Hall [9]
	1.95–2.2	P^{sat}	1.5	12	Escobedo and de Pablo [14]
	1.5–4.0	0.501–7.682	1.5	14	Tavares et al. [13]
				47	
32-Mer	2.15–2.41	P^{sat}	1.5	10	Escobedo and de Pablo [14]
				10	
100-Mer	3.0	0.057–4.531	1.5	4	Escobedo and de Pablo [14]
	2.35–2.41	P^{sat}	1.5	6	Escobedo and de Pablo [14]
				10	
Total N				370	

The values of k_1 to k_7 were determined from fitting to the simulation results of hard-sphere molecules and square-well monomers (with $m = 1$). With the optimal values of $k_1 = 3.453667$, $k_2 = 1.610016$, $k_3 = -1.57253$, $k_6 = -16.504144$, $k_7 = 21.443081$, Eqs. (4) and (5) represent the properties of hard spheres and square-well monomers well [47].

4.2. Contribution of square-well chain formation

The compressibility factors for square-well chain formation is calculated by adding the reference hard-sphere chain formation, $Z_{hs,cf}$, term to a perturbation term, $Z_{sw,cf,pert}$:

$$Z_{sw,cf} = Z_{hs,cf} + Z_{sw,cf,pert} \quad (6)$$

The expression for $Z_{hs,cf}$ is taken from the first-order thermodynamic perturbation theory of Wertheim (TPT1) [48],

$$Z_{hs,cf} = (1-m)\frac{2.5\eta - \eta^2}{(1-\eta)(1-0.5\eta)} \quad (7)$$

The perturbation term, $Z_{sw,cf,pert}$, is formulated as an empirical function in terms of the reduced temperature and reduce density:

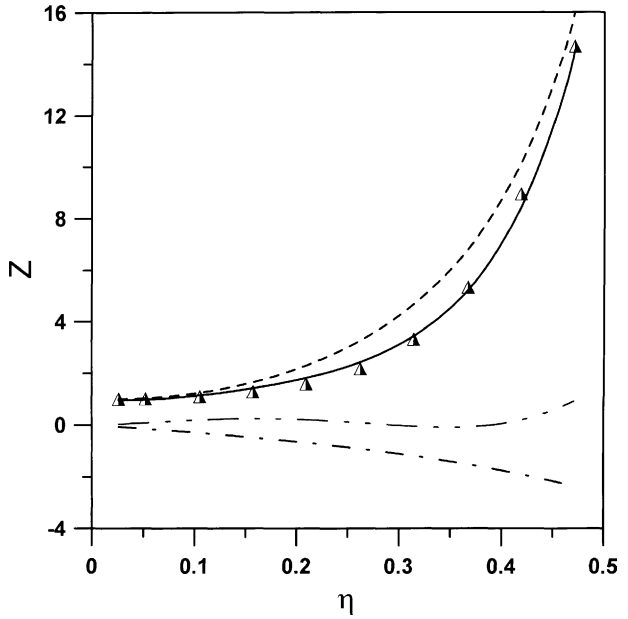

Figure 7. Comparison of the calculated compressibility factor from theory (solid line) and simulation (Δ) [13] for the square-well dimer fluid at $T^* = 3.0$. Also shown are the individual contributions: $Z_{sw,nb}$ (dashed), $Z_{hs,cf}$ (dot-dashed) and $Z_{sw,cf,pert}$ (dot–dot-dashed).

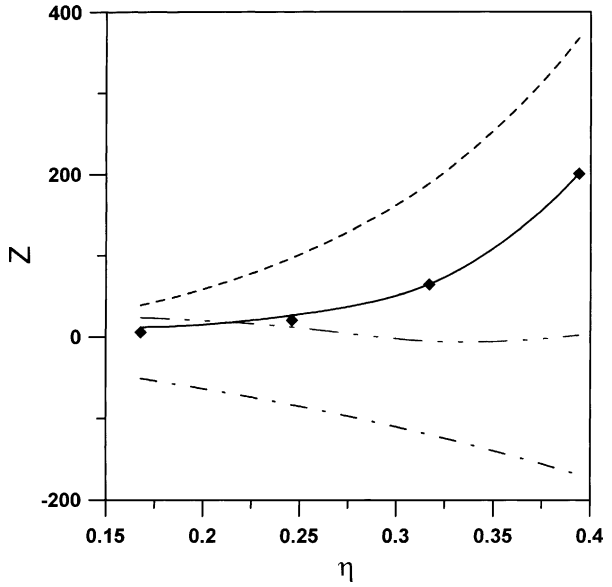

Figure 8. Comparison of the calculated compressibility factor from theory (solid line) and simulation (◆) [14] for the square-well 100-mer fluid at $T = 3.0$. Also shown are the individual contributions: $Z_{sw,nb}$ (dashed), $Z_{hs,cf}$ (dot-dashed) and $Z_{sw,cf,pert}$ (dot–dot-dashed).

$$Z_{sw,cf,pert} = (1-m)\left[\frac{1}{T^*}(a_1\eta + a_2\eta^2 + a_3\eta^3 + a_4\eta^4) + \frac{a_5\eta}{T^{*2}} + \frac{a_6\eta}{T^{*3}}\right] \quad (8)$$

Note that the dependence on m is consistent with SAFT. Introducing Eqs. (3)–(8) into Eq. (1) gives the new equation of state for square-well chain molecules as:

$$\begin{aligned} Z &= 1 + m[(Z_{hs} - 1) + Z_{sw,att}] \\ &\quad + (1-m)(Z_{hs,cf} + Z_{sw,cf,pert}) \\ &= 1 + m\left\{\frac{(k_1+k_2)\eta}{1-k_2\eta} + (\lambda - 0.5)^{3/2} \times \left[\frac{k_6\eta + k_7\eta^2}{T^*(1-k_2\eta)(1-k_3\eta)}\right]\right\} \\ &\quad + (1-m)\frac{2.5\eta - \eta^2}{(1-\eta)(1-0.5\eta)} \\ &\quad + (1-m)\left[\frac{1}{T^*}(a_1\eta + a_2\eta^2 + a_3\eta^3 + a_4\eta^4) + \frac{a_5\eta}{T^{*2}} + \frac{a_6\eta}{T^{*3}}\right] \end{aligned} \quad (9)$$

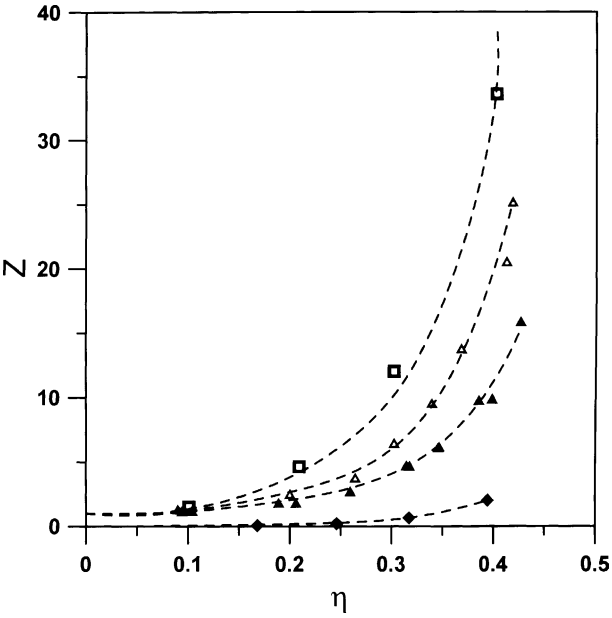

Figure 9. Comparison of the calculated compressibility factors (dashed line) with simulation results for square-well 4-mer (▲) [14], 8-mer (△) [14], 16-mer (◘) [13] and 100-mer (◆, y-scale $= Z/100$) [14] fluids at $T^* = 3.0$.

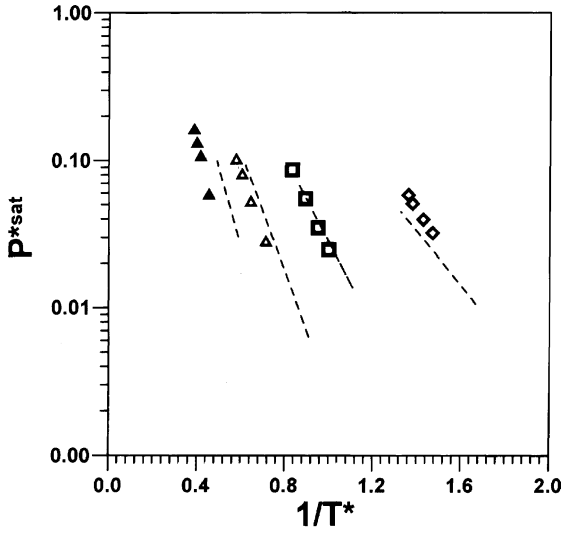

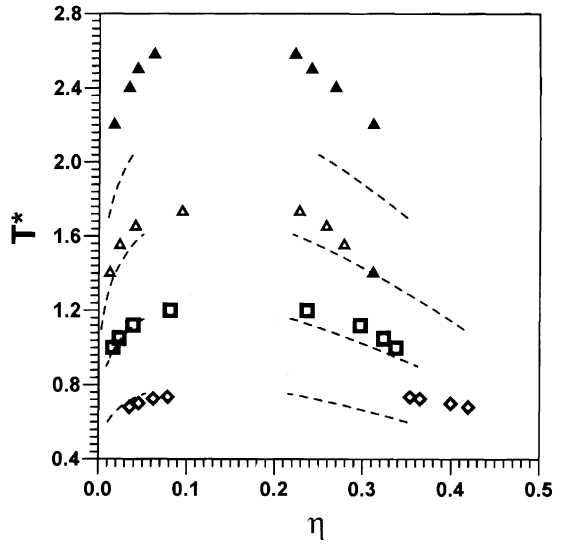

Figure 10. Comparison of the calculated T^*–η phase envelopes and vapor pressures from the new equation of state (dashed line) with the simulation results for square-well monomer [22] of $\lambda = 2.0$ (▲), $\lambda = 1.75$ (△), $\lambda = 1.5$ (◘), and $\lambda = 1.25$ (◇).

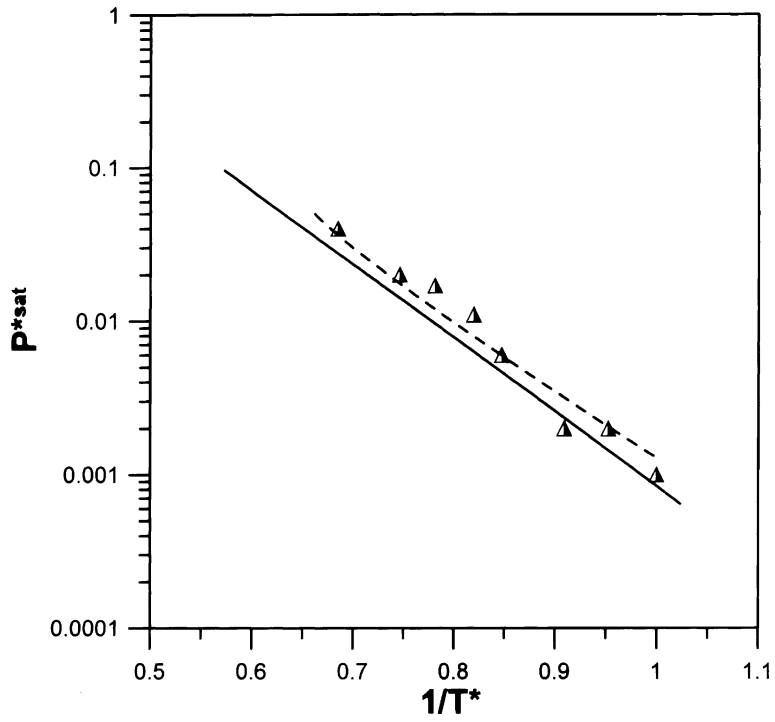

Figure 11. Comparison of the calculated vapor pressures from the new equation of state (dashed line) and the SAFT-VR equation (solid line) with simulation results (▲) [17] for square-well dimer fluid.

The coefficients, a_1 to a_6, in the above equation were obtained by fitting the model to the MC simulation data of square-well chain molecules with the following objective function, Δ:

$$\Delta = \sum_{i=1}^{n_p} |P^*_{i\text{calc}} - P^*_{i\text{siml}}| \tag{10}$$

where n_p is the number of data points. In total, 370 MC data points are used in the parameter determination. The information from these data sources is summarized in Table 6. With the optimal values of $a_1 = -2.393582$, $a_2 = -82.311554$, $a_3 = 543.897526$, $a_4 = -821.080818$, $a_5 = 2.342257$, $a_6 = -2.847097$, the new model correlates the *PVT* simulation data to an average absolute deviation (AAD) of 0.142 for P^* and 0.440 for the compressibility factor, Z.

Figures 7 and 8 present the predicted compressibility factors, including individual contributions, from this new equation of state at $T^* = 3.0$ for the dimer and 100-mer fluids, respectively. The calculated compressibility factors agree well with the MC simulation results for both chain fluids over the entire density range. These two graphs show that the contribution of non-bonded square-well segments is the dominant term, and that the hard-sphere chain formation term is a negative contribution (attraction). Although the magnitude of the perturbation due to square-well chain formation is relatively small compared to the other terms, this correction term is the key to obtaining accurate results. Good agreement between the theoretical predictions and simulation data is also shown in Figure 9, which compares the calculated compressibility factors with the MC simulation results for 4-mer, 8-mer, 16-mer, and 100-mer fluids at $T^* = 3.0$. The new equation quantitatively represents the *PVT* behavior of square-well chain molecules over a diverse range of conditions, except in the region near the critical point. This new equation is also applicable to the square-well chain molecules with variable well-width, as shown in Figures 5 and 6.

In addition to volumetric property calculation, the new equation is also applied to vapor–liquid equilibrium (VLE) prediction. At a given T^*, the reduced densities of the coexistence phases (η_{vap} and η_{liq}) are determined from the following simultaneous equations:

$$P^*(T^*, \eta_{\text{vap}}) = P^*(T^*, \eta_{\text{liq}}) \tag{11}$$

$$\mu_{\text{vap}}(T^*, \eta_{\text{vap}}) = \mu_{\text{liq}}(T^*, \eta_{\text{liq}}) \tag{12}$$

or

$$\ln \eta_{\text{vap}} + \frac{\mu^{\text{E}}_{\text{vap}}}{kT} = \ln \eta_{\text{liq}} + \frac{\mu^{\text{E}}_{\text{liq}}}{kT} \tag{13}$$

where the expression of the excess chemical potential (μ^{E}) for the proposed equation of state is given by

$$\frac{\mu^{\text{E}}}{kT} = \int_{\eta=0}^{\eta} \frac{Z-1}{\eta} \mathrm{d}\eta + Z - 1$$
$$= \frac{m(k_1+k_2)}{k_2} \ln\left(\frac{1}{1-k_2\eta}\right) + \frac{m(\lambda-0.5)^{3/2}}{T^*(k_2-k_3)}$$
$$\times \left[k_6 \ln\left(\frac{1-k_3\eta}{1-k_2\eta}\right) - \frac{k_7}{k_2} \ln(1-k_2\eta)\right.$$

$$+\frac{k_7}{k_3}\ln(1-k_3\eta)\Bigg]+(1-m)\ln\left[\frac{1-0.5\eta}{(1-\eta)^3}\right]$$
$$+(1-m)\left[\left(\frac{a_1}{T^*}+\frac{a_5}{T^{*2}}+\frac{a_6}{T^{*3}}\right)\eta+\frac{a_2}{2T^*}\eta^2\right.$$
$$\left.+\frac{a_3}{3T^*}\eta^3+\frac{a_4}{4T^*}\eta^4\right]+Z-1 \quad (14)$$

Once the coexisting densities have been determined, the corresponding vapor pressure is readily obtained from Eq. (11). Figure 10 compares the calculated vapor pressure, saturated vapor and liquid densities with the simulation results of del Rio et al. [22] for the square-well monomer of variable range. We note that this simulation data was not included in the fitting process. The new model accurately represents the saturated properties for the square-well monomer for λ=1.25–1.75, but underestimates the critical properties of the square-well monomer with λ = 2.0. Figure 11 compares the predicted vapor pressures with the MC simulation data for square-well dimers. Figure 12 presents T^*–η phase envelopes for the dimer fluid to the 100-mer fluid. From the figure we can see there is good agreement between the new equation of state and the simulation data. For comparison we include the predictions of the SAFT-VR EOS [32], which is seen to overestimate the critical temperatures. However, this is to be expected for a classical equation of state which is analytical in the free energy and no attempt has been made to optimize the agreement between the SAFT-VR EOS and the simulation results. This agreement could be improved by using a higher order perturbation theory in deriving the properties of the square-well fluid or by incorporating the non-analytical behavior seen at the critical point of real fluids as in the SAFT-VRX EOS [49,50]. For the new model, good agreement is observed in the critical region for both the dimer and 4-mer fluids. For example, the critical point of 4-mer fluid was estimated at the reduced temperature of 1.81 and the reduced density of 0.175, while the simulation result was at 1.90 and 0.134, respectively. The saturated vapor pressures and the critical density, however, were underestimated for longer chains.

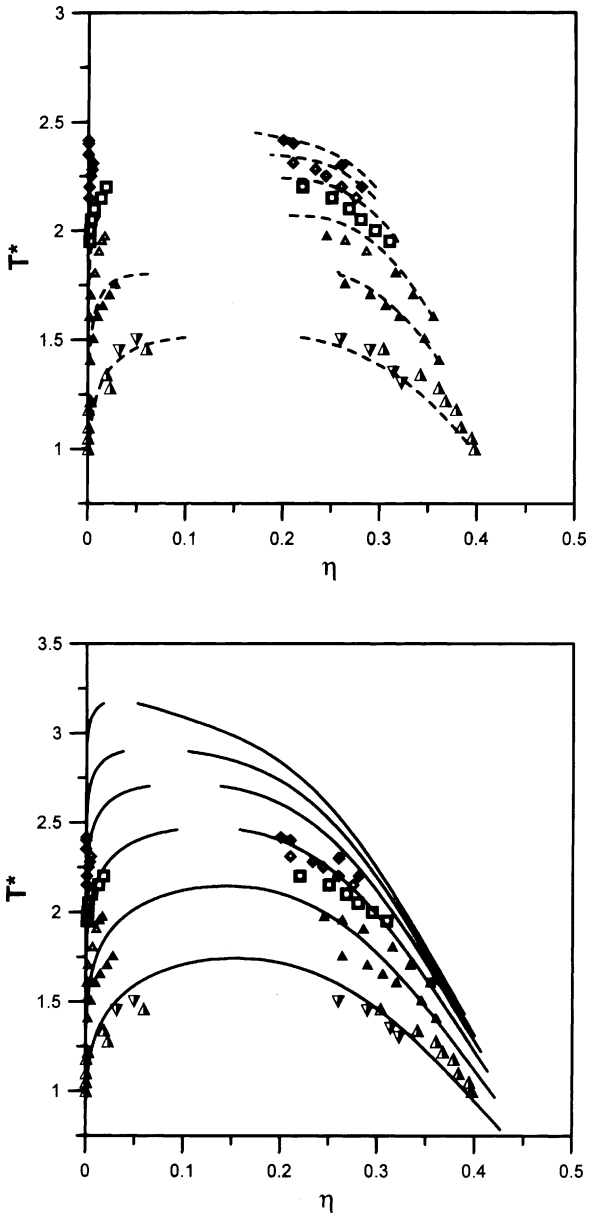

Figure 12. Comparison of the calculated T^*–η phase envelopes from the new equation of state (top half, dashed curves) and the SAFT-VR equation (bottom half, solid curves) with simulation results for square-well dimer (▲, ▽) [8,17], 4-mer (▲) [14], 8-mer (△) [14], 16-mer (□) [14], 32-mer (◆) [14] and 100-mer (◆) [14] fluids.

5. Conclusions

The volumetric properties of square-well chain molecules have been determined from MC simulation using the NPT ensemble for the dimer, 4-mer, 8-mer, and 16-mer fluids at temperatures near or below the critical point. *PVT* diagrams were presented for the square-chain fluids studied and comparisons made with simulation data taken from the literature. A new equation was developed for square-well chain molecules, based on the available MC data. In general, this new equation is capable of describing quantitatively the *PVT* behavior for square-well chain fluids over a wide range of conditions. Excellent results were also obtained for the vapor–liquid equilibrium calculations for the dimer and 4-mer molecules. The new equation, however, underestimates the saturated pressures for chain molecules, longer than eight.

List of symbols

a_i	coefficients
k	Boltzmann's constant
k_i	coefficients
m	chain length (number of segment)
n_p	number of data points
N	number of molecule
P	pressure
P^*	reduced pressure

T	temperature
T^*	reduced temperature
V	volume
Z	compressibility factor

Greek letters

σ	hard core diameter
Δ	objective function
ρ	number density of segment
ε	characteristic attraction energy
λ	dimensionless well width
η	reduced density
μ	chemical potential

Subscripts

att	attractive
cf	chain formation
hs	hard-sphere
liq	liquid phase
nb	non-bounded
pert	perturbation
sw	square-well
vap	vapor phase

Superscripts

calc	calculated value
E	excess property
sat	saturated
siml	simulation

Acknowledgements

MJL acknowledges financial support from the National Science Council, ROC, through Grant no. 39179F. CMC and PTC were supported by the Division of Chemical Sciences, Geosciences, and Biosciences, Office of Basic Energy Sciences, U.S. Department of Energy, under grant FG05-94ER14421 to Vanderbilt University. This research used resources of the Scalable Intracampus Research Grid (SInRG) Project at the University of Tennessee supported by the National Science Foundation CISE Research Infrastructure Award EIA-9972889.

References

[1] R. Dickman, C.K. Hall, J. Chem. Phys. 85 (1986) 4108–4115.
[2] R. Dickman, C.K. Hall, J. Chem. Phys. 89 (1988) 3168–3174.
[3] J. Gao, J.H. Weiner, J. Chem. Phys. 91 (1989) 3168–3173.
[4] M.A. Denlinger, C.K. Hall, Mol. Phys. 71 (1990) 541–559.
[5] T. Boublik, C. Vega, M. Diaz-Pena, J. Chem. Phys. 93 (1990) 730–736.
[6] A.L. Archer, G. Jackson, Mol. Phys. 74 (1991) 881–896.
[7] M.D. Amos, G. Jackson, Mol. Phys. 74 (1991) 191–210.
[8] A. Yethiraj, C.K. Hall, Mol. Phys. 72 (1991) 619–641.
[9] A. Yethiraj, C.K. Hall, J. Chem. Phys. 95 (1991) 1999–2005.
[10] A. Yethiraj, C.K. Hall, J. Chem. Phys. 95 (1991) 8494–8506.
[11] C.K. Hall, A. Yethiraj, J.M. Wichert, Fluid Phase Equilib. 83 (1993) 313–322.
[12] J.M. Wichert, C.K. Hall, Macromolecules 27 (1994) 2744–2756.
[13] F.W. Tavares, J. Chang, S.I. Sandler, Mol. Phys. 86 (1995) 1451–1471.
[14] F.A. Escobedo, J.J. de Pablo, Mol. Phys. 87 (1996) 347–366.
[15] F.W. Tavares, J. Chang, S.I. Sandler, Fluid Phase Equilib. 140 (1997) 129–143.
[16] H.S. Gulati, C.K. Hall, J. Chem. Phys. 107 (1997) 3930–3946.
[17] L.A. Davies, A. Gil-Villegas, G. Jackson, S. Calero, S. Lago, Phys. Rev. E 57 (1998) 2035–2044.
[18] B.J. Zhang, S. Liang, Y. Lu, Fluid Phase Equilib. 180 (2001) 183–194.
[19] M.L.L. Paredes, R. Nobrega, F.W. Tavares, Fluid Phase Equilib. 179 (2001) 245–267.
[20] C. McCabe, A. Gil-Villegas, G. Jackson, Chem. Phys. Lett. 303 (1999) 27–36.
[21] C. McCabe, A. Gil-Villegas, G. Jackson, F. del Rio, Mol. Phys. 97 (1999) 551–558.
[22] F. del Rio, E. Avalos, R. Espindola, L.F. Rull, G. Jackson, S. Lago, Mol. Phys. 100 (2002) 2531–2546.
[23] X.Y. Wang, Y.C. Chiew, J. Chem. Phys. 115 (2001) 4376–4386.
[24] C. McCabe, Y.V. Kalyuzhnyi, P.T. Cummings, Fluid Phase Equilib. 194–197 (2002) 185–196.
[25] Y.V. Kalyuzhnyi, C. McCabe, P.T. Cummings, G. Stell, Mol. Phys. 100 (2002) 2499–2517.
[26] W.G. Chapman, K.E. Gubbins, G. Jackson, M. Radosz, Fluid Phase Equilib. 52 (1989) 31–38.
[27] W.G. Chapman, K.E. Gubbins, G. Jackson, M. Radosz, Ind. Eng. Chem. Res. 29 (1990) 1709–1721.
[28] I.G. Economou, Ind. Eng. Chem. Res. 41 (2002) 953–962.
[29] E.A. Muller, K.E. Gubbins, Ind. Eng. Chem. Res. 40 (2001) 2193–2211.
[30] S.H. Huang, M. Radosz, Ind. Eng. Chem. Res. 29 (1990) 2284–2294.
[31] S.H. Huang, M. Radosz, Ind. Eng. Chem. Res. 30 (1991) 1994–2005.
[32] A. Gil Villegas, A. Galindo, P.J. Whitehead, S.J. Mills, G. Jackson, A.N. Burgess, J. Chem. Phys. 106 (1997) 4168–4186.
[33] H. Adidharma, M. Radosz, Fluid Phase Equilib. 160 (1999) 165–174.
[34] M.S. Yeom, J. Chang, H. Kim, Kor. J. Chem. Eng. 17 (2000) 52–57.
[35] J.C. Tsai, Y.P. Chen, Fluid Phase Equilib. 187 (2001) 39–59.
[36] M. Banaszak, Y.C. Chiew, M. Radosz, Phys. Rev. E 48 (1993) 3760–3765.
[37] J.W. Jiang, J.M. Prausnitz, J. Chem. Phys. 111 (1999) 5964–5974.
[38] J. Gross, G. Sadowski, Fluid Phase Equilib. 168 (2000) 183–199.
[39] M.L.L. Paredes, R. Nobrega, F.W. Tavares, Fluid Phase Equilib. 179 (2001) 231–243.
[40] J.A. Barker, D. Henderson, Rev. Mod. Phys. 48 (1976) 587.
[41] M.S. Wertheim, J. Stat. Phys. 35 (1984) 19–34.
[42] M.S. Wertheim, J. Stat. Phys. 35 (1984) 35–47.
[43] M.S. Wertheim, J. Stat. Phys. 42 (1986) 459–476.
[44] M.S. Wertheim, J. Stat. Phys. 42 (1986) 477–492.
[45] C. McCabe, A. Gil-Villegas, G. Jackson, Chem. Phys. Lett. 303 (1999) 27–36.
[46] D. Frenkel, B. Smit, Understanding Molecular Simulations: From Algorithms to Applications, Academic Press, 1996.
[47] H.M. Lin, J.T. Chen, M.J. Lee, Fluid Phase Equilib. 126 (1996) 29–52.
[48] M.S. Wertheim, J. Chem. Phys. 87 (1987) 7323–7331.
[49] C. McCabe, S.B. Kiselev, Fluid Phase Equilib. 219 (2004) 3–9.
[50] C. McCabe, S.B. Kiselev, Ind. Eng. Chem. Res. (in press).